Geochemistry Geophysics Geosystems G3
AN ELECTRONIC JOURNAL OF THE EARTH SCIENCES
Published by AGU and the Geochemical Society

Article
Volume 10, Number 6
18 June 2009
Q06T06, doi:10.1029/2009GC002388
ISSN: 1525-2027

January 2006 seafloor-spreading event at 9°50′N, East Pacific Rise: Ridge dike intrusion and transform fault interactions from regional hydroacoustic data

Robert P. Dziak
CIMRS, Oregon State University, 2115 Southeast OSU Drive, Newport, Oregon 97365, USA

Pacific Marine Environmental Laboratory, NOAA, 2115 Southeast OSU Drive, Newport, Oregon 97365, USA (robert.p.dziak@noaa.gov)

Delwayne R. Bohnenstiehl
Department of Marine, Earth and Atmospheric Sciences, North Carolina State University, Campus Box 8208, Raleigh, North Carolina 27695, USA

Haruyoshi Matsumoto, Matthew J. Fowler, and Joseph H. Haxel
CIMRS, Oregon State University, 2115 Southeast OSU Drive, Newport, Oregon 97365, USA

Pacific Marine Environmental Laboratory, NOAA, 2115 Southeast OSU Drive, Newport, Oregon 97365, USA

Maya Tolstoy and Felix Waldhauser
Lamont-Doherty Earth Observatory, Earth Institute at Columbia University, 61 Route 9W, Palisades, New York 10964-8000, USA

[1] An array of autonomous underwater hydrophones is used to investigate regional seismicity associated with the 22 January 2006 seafloor-spreading event on the northern East Pacific Rise near 9°50′N. Significant earthquake activity was observed beginning 3 weeks prior to the eruption, where a total of 255 earthquakes were detected within the vicinity of the 9°50′N area. This was followed by a series of 252 events on 22 January and a rapid decline to background seismicity levels during the subsequent 3 days. Because of their small magnitudes, accurate locations could be derived for only 20 of these events, 18 of which occurred during a 1-h period on 22 January. These earthquakes cluster near 9°45′N and 9°55′N, at the distal ends of the young lava flows identified posteruption, where the activity displays a distinct spatial-temporal pattern, alternating from the north to the south and then back to the north. This implies either rapid bilateral propagation along the rift or the near-simultaneous injection of melt vertically from the axial magma lens. Short-duration *T* wave risetimes are consistent with the eruption of lavas in the vicinity of 9°50′N on 22 January 2006. Eruptions on 12 and 15–16 January also may be inferred from the risetime data; however, the locations of these smaller-magnitude events cannot be determined accurately. Roughly 15 h after the last earthquakes were located adjacent to the eruption site, a sequence of 16 earthquakes began to the north-northeast at a distance of 25–40 km from the 9°50′N site. These events are located in vicinity of the Clipperton Transform and its western inside corner, an area from which the regional hydrophone network routinely detects seismicity. Coulomb stress modeling indicates that a dike intrusion spanning the known eruptive zone to the south (9°46′–9°56′N) would act to promote normal faulting or a combination of normal faulting and transform slip within this region, with stress changes on the order of 1–10 kPa.

Components: 8051 words, 7 figures, 1 table.

Keywords: mid-ocean ridge; fast spreading; earthquakes; magma intrusion; hydroacoustics; hydrophone.

Index Terms: 8416 Volcanology: Mid-oceanic ridge processes (1032, 3614); 8414 Volcanology: Eruption mechanisms and flow emplacement; 7280 Seismology: Volcano seismology (8419).

Received 16 January 2009; **Revised** 11 May 2009; **Accepted** 14 May 2009; **Published** 18 June 2009.

Dziak, R. P., D. R. Bohnenstiehl, H. Matsumoto, M. J. Fowler, J. H. Haxel, M. Tolstoy, and F. Waldhauser (2009), January 2006 seafloor-spreading event at 9°50′N, East Pacific Rise: Ridge dike intrusion and transform fault interactions from regional hydroacoustic data, *Geochem. Geophys. Geosyst.*, *10*, Q06T06, doi:10.1029/2009GC002388.

Theme: Recent Volcanic Eruptions, Properties, and Behavior of the Fast Spreading East Pacific Rise at 8°–11°N
Guest Editors: S. M. Carbotte, R. Haymon, and W. Seyfield

1. Introduction

[2] Seafloor dike injection events along the global mid-ocean ridge system are the fundamental process for creation of ocean crust; yet, these events are rarely observed because of the remoteness of the deep ocean. The first studies of MOR diking/eruptive events and seafloor eruptions in the Pacific were serendipitous, occurring during ongoing studies of the Juan de Fuca Ridge and East Pacific Rise [*Haymon et al.*, 1993; *Baker et al.*, 1995]. Much of what is now known about the active processes associated with dike injection comes from the remote detection of seismicity triggered as magma is injected into the upper crust. This monitoring is accomplished typically using a combination of global seismic stations [e.g., *Tolstoy et al.*, 2001], local OBS arrays [e.g., *Sohn et al.*, 1998], or regional hydrophone arrays [e.g., *Dziak et al.*, 1995]. The earthquake data presented in these studies cover the range from ultraslow to fast spreading ridges and have been used to elucidate the speed and dynamics of magma injection processes, as well as provide insights into how injection dynamics influences hydrothermal fluid release and the eruption of lava onto the seafloor.

[3] Since May 1996, an array of six autonomous underwater hydrophones (AUH) has been deployed along the fast spreading East Pacific Rise (EPR, 110 mm/a) [*Fox et al.*, 2001]. The hydrophones detect seismically generated Tertiary (*T*) waves that propagate efficiently within the ocean's low-velocity waveguide [*Fox et al.*, 1995, 2001]. The array effectively monitors the plate boundary between approximately 10°S and 10°N, providing a complete catalog of $m_b > 2.5$ earthquakes [*Fox et al.*, 2001; *Bohnenstiehl et al.*, 2002] (Figure 1). Throughout its history, several small earthquake swarms have been detected along the otherwise aseismic spreading center [*Fox et al.*, 2001; *Bohnenstiehl et al.*, 2003]. These sequences typically contain no more than a few tens of locatable earthquakes occurring over a period of a several hours, and have rarely included any events large enough to be detected by distant land-based seismic stations. In the year 2000, a research cruise was organized to investigate several of these sites [*Fornari et al.*, 2000]. However, clear evidence associating these swarms with dike intrusions and/or seafloor eruptions was not found during this cruise, and presently there are few observational constraints on the dynamics of magma emplacement at fast spreading rates.

[4] The well-studied 9°50′N hydrothermal field [e.g., *Haymon et al.*, 1993; *Fornari et al.*, 1998] lies along the northern boundary of the region monitored by the AUH array. In 1991, the immediate aftermath of a seafloor eruption was discovered at this site during a series of Alvin dives [*Haymon et al.*, 1993]. Recognizing an opportunity to explore the geological and biological evolution of the site posteruption, researchers initiated a series of long-term, interdisciplinary studies. The Ridge 2000 Program subsequently designated the area as a site of focused study, and in January 2006, following nearly 15 years of quiescence, this section of the ridge crest experienced another seafloor eruption [*Tolstoy et al.*, 2006; *Soule et al.*, 2007]. A local Ocean Bottom Seismic (OBS) network captured this event; however, lava engulfed most of the

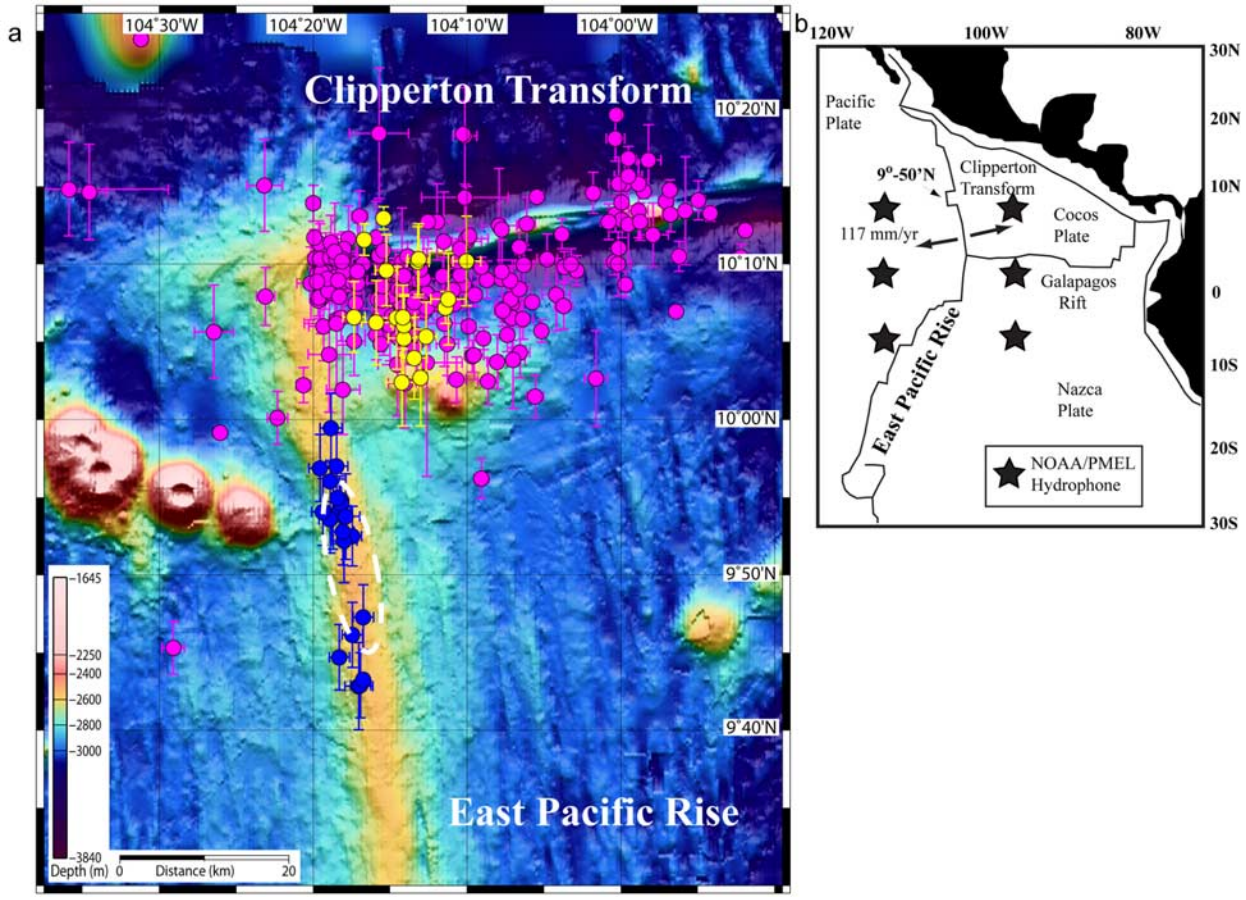

Figure 1. (a) Bathymetric map of the East Pacific Rise, showing earthquakes located during dike injection of January 2006. Blue dots are earthquakes detected and located during inferred eruption day of 22 January 2006. Red dots are earthquakes located in the region from May 1996 until 21 January 2006, and yellow dots are post 22 January. Error bars are 68% confidence interval. Dashed line shows mapped location of new lava flows from the eruption. (b) Location of EPR within the eastern equatorial Pacific and location of hydrophone moorings (black stars).

stations and it was not possible to estimate earthquake hypocenters [*Tolstoy et al.*, 2006].

[5] Here we describe the regional hydrophone records of seismicity bracketing the time of the 9°50′N eruption, and compare the space-time characteristics of the earthquakes from this episode of seafloor spreading to previous swarms recorded by the equatorial Pacific and other regional hydrophone arrays. This assessment complements OBS observations of the 9°50′N activity and further elucidates the dynamics of a rarely observed episode of seafloor spreading.

2. Hydrophone Monitoring and Acoustic Propagation

[6] A schematic diagram of the autonomous hydrophone instrument and mooring is shown in Figures 2a and 2b. The hydrophone instrument package includes a single ceramic hydrophone, a filter/amplifier stage, accurate clock, and processor modified from off-the-shelf hardware (Figure 2a). The instrument records at 16-bit data resolution at 250 Hz (1–110 Hz band pass) for periods of up to 2.5 years. The hydrophone and preamplifier together have a flat frequency response over the passband, but roll-off begins at frequencies <0.6 Hz. The hydrophones were each deployed with a 60-Gb hard drive for data storage. A temperature-correcting crystal oscillator with an average drift of 400 ms a^{-1} provides accurate timing during the typical 1–2 year deployment duration. The analog filter/amplifier section is designed to prewhiten the ocean ambient noise spectrum. The electronics are powered by 168 standard alkaline D-cell batteries, which are replaced on the research vessel during redeployments.

[7] The field package includes a custom pressure case manufactured from aircraft titanium tubing,

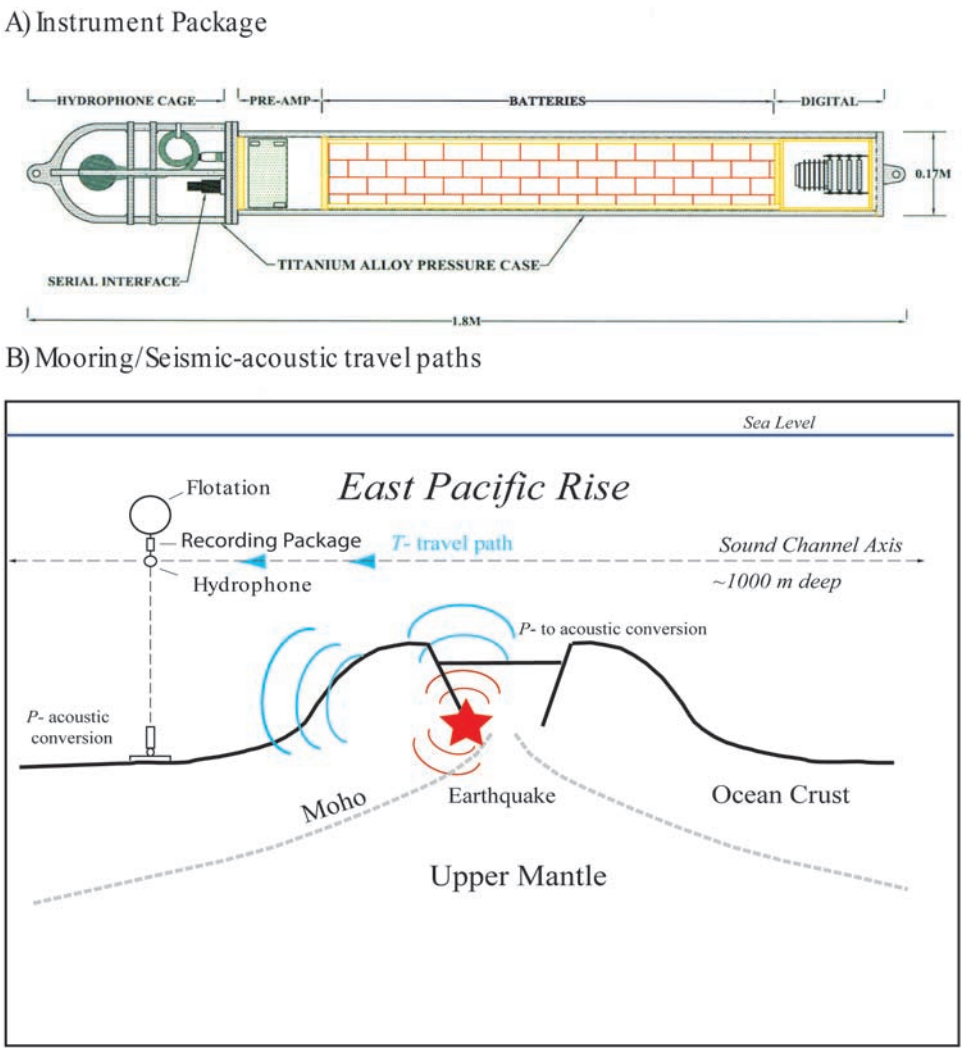

Figure 2. Diagram showing (a) hydrophone schematics and (b) mooring design and probable seismic/acoustic propagation paths detected on the hydrophones. Preamplifier, digital logging section, and hard drives are contained within a titanium pressure case powered by 150 D-cell batteries. The hydrophone instrument package is anchored to the seafloor then suspended in the SOFAR channel using a single large syntactic float. Earthquakes from East Pacific Rise produce seismic waves that propagate upward and laterally through the crust and convert to an acoustic phase at the seafloor-ocean interface. This acoustic phase will then propagate into the sound channel waveguide becoming a *T* wave [*Park and Odom*, 2001].

which can be deployed to depths of 1200 m. The instrument case is attached to a standard oceanographic mooring (Figure 2b) with anchor, acoustic release, premeasured mooring line, and a syntactic foam float to place the sensor at the proper water depth within the ocean sound channel. A small pressure and temperature recorder is attached to the mooring line below the float to record the depth should dramatic hydrophone depth changes occur in response to stronger than normal currents.

[8] Typically, a submarine earthquake will produce seismic waves that propagate through the shallow ocean crust and convert to an acoustic phase (*T* wave) at the seafloor-ocean interface. Since acoustic *T* waves propagate laterally in the ocean sound channel, they obey cylindrical spreading (r^{-1}) energy loss as opposed to the spherical spreading (r^{-2}) of solid earth seismic *P* and *S* waves. Consequently, sound channel hydrophones can often detect smaller ($m_b >$ 2.5) and therefore more numerous earthquakes than land-based seismic networks [*Dziak et al.*, 2004]. OBS sensors, however, remain the preferred technology for monitoring local seismicity associated with ridge axis hydrothermal systems and magma lenses. Temporary deployments of OBS instruments along the axis reveal that 100–1000 s of otherwise undetected microearthquakes ($M_L < 2$) may be produced annually per kilometer of ridge

crest [e.g., *Sohn et al.*, 1998; *Tolstoy et al.*, 2006, 2008].

3. OBS, Water Column, and Seafloor Observations of the January 2006 Eruption

[9] In October 2003, an OBS monitoring program was initiated at the EPR 9°50′N integrated study site [*Tolstoy et al.*, 2006, 2008]. The experiment, which continued through April 2007, consisted of four consecutive free-fall deployments of 7–12 short-period OBSs. The array spanned a 4 × 4 km area surrounding the site's well-studied hydrothermal system, between 9°49′ and 9°51′N.

[10] During a recovery cruise on 25 April 2006, only 4 of the 12 OBS instruments were retrieved from the seafloor [*Tolstoy et al.*, 2006]. Five of the OBS would not respond to acoustic release commands, while three were acknowledging acoustic release codes but did not leave the seafloor. Given these unusual circumstances, an eruption was immediately suspected to have occurred since the last OBS servicing in early 2005.

[11] Corroborating evidence for the eruption came from anomalies in water column measurements of temperature and light scattering made during the servicing cruise and on a subsequent response cruise [*Tolstoy et al.*, 2006; *Cowen et al.*, 2007]. Seafloor images confirmed the existence of new lava flows and constrained the eruption's spatial extent, which appears to have mirrored that of the 1991 eruptive episode [*Haymon et al.*, 1993]. Lava flow morphologies indicate the highest effusion rates were between 9°49′N and 9°52′N, with lava extending between 9°46′–9°56′N [*Tolstoy et al.*, 2006; *Soule et al.*, 2007]. Radiometric dating of rocks collected from the "young" terrain indicate that most lavas may have been emplaced as early as June–July 2005 [*Rubin et al.*, 2008]. These earlier effusion dates may be correlated to periods of slighted enhanced seismicity recorded on the OBSs [*Rubin et al.*, 2008]; however, the seismic energy release rate during this period is dwarfed by that observed on 22 January [*Tolstoy et al.*, 2006]. Temperature records from high-temperature "M" Vent at 9°51.6′N shows a sudden >208°C drop in temperature on 11 January 2006 that remains until a rapid 228°C increase on 28 January 2006, indicative of a major reorganization of hydrothermal fluid circulation during this 17 day period (K. Von Damm et al., Vent fluid temperature time-series data and correlative data pre- and post-eruption for high-temperature hydrothermal vents at the East Pacific Rise 9°50′N, manuscript in preparation, 2009).

[12] As waveform records initially could be retrieved from only two of the four recovered OBSs, the local seismic observations provided limited location capability. However, an important temporal record of local seismicity was supplied through the analysis of short-period (5–25 Hz) seismic energy release and automated event detection rates [*Tolstoy et al.*, 2006]. The seismic records were dominated by a single period of intense activity, which began at 1345 UT on 22 January 2006 and continued for approximately 6 h. During this time, earthquake detection rates exceeding 250 events/h were recorded on the OBSs. *Tolstoy et al.* [2006] interpreted this activity as marking the propagation of the primary dike that fed the eruption. Microearthquake *S-P* times from the two surviving OBS stations suggested that events were concentrated near 9°50.5′N during the first hour, then disperse during the remaining 5 h.

[13] For 1 h, beginning at 1445 UT, seismic amplitudes peaked at levels five times higher than at other times during the 6-h period. *Tolstoy et al.* [2006] interpreted this period to coincide with the dike rising to the surface from the axial magma chamber depth of ∼1.4 km, implying a vertical propagation rate of ∼0.38 m/s. During the weeks following the inferred diking event, the level of microseismic activity tapered off rapidly, reaching background rates far less than the over 1000 events/d commonly observed in the months preceding the spreading episode.

4. Hydroacoustic Observations

4.1. Dike Injection Seismicity

[14] The EPR hydrophone array was recovered in December 2006, with 2 years of continuous waveform data recorded by each of the six instruments. The hydrophones detected 2–3 earthquakes from the vicinity of 9°50′N between January and December 2005, 255 earthquakes from the 9°50′N area in the 3 weeks prior to 22 January (the inferred day of the eruption), then 252 events on 22 January, after which earthquake counts rapidly declined to background levels in less than 3 days (Figure 3). No evidence of volcanic tremor associated with the January 2006 earthquake swarm was recorded on the hydrophone array. As *Tolstoy et al.* [2006] observed, the peak seismic activity (and likely the

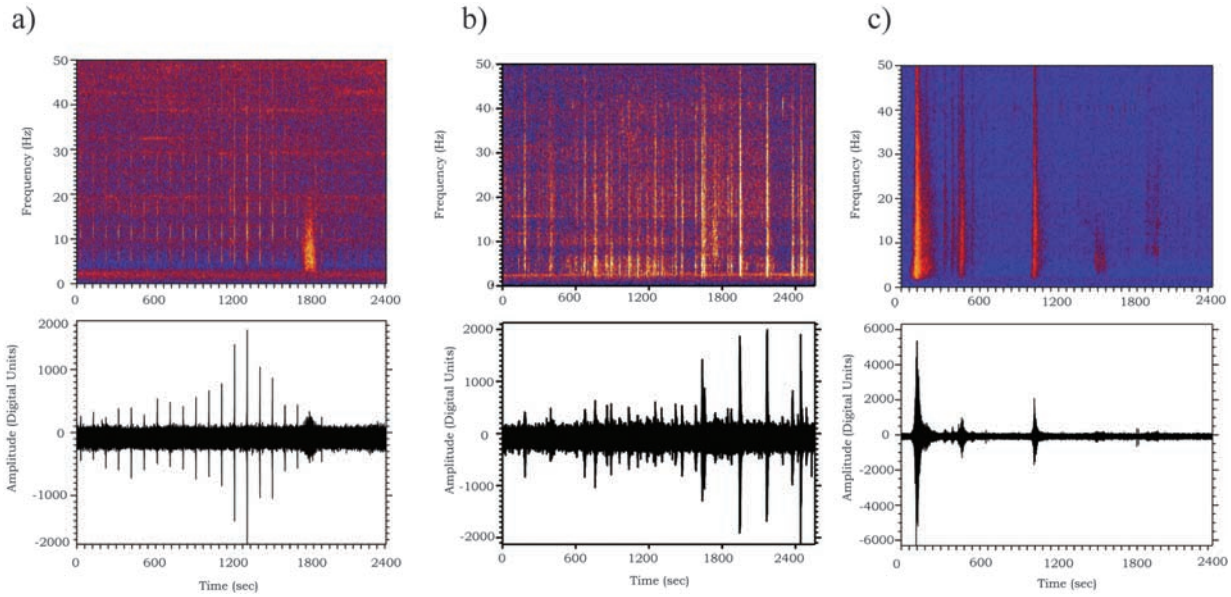

Figure 3. The time series and spectrogram of the northeast hydrophone from (a) 2300 UT on 15–16 January, (b) 1500 UT on 22 January, and (c) 1030 UT on 23 January 2006. Earthquakes are impulsive, broadband signals. Much of the low-frequency (<3 Hz) component of the earthquake acoustic energy is missing from these events, likely because of attenuation affects from the physical dimensions (~400 m) of the sound channel in the equatorial Pacific ocean. Overall, the seismicity from 15 to 16 and 22 January (on the ridge axis) exhibits lower-amplitude, shorter-duration *T* wave codas compared to the seismicity on 23 January that occurred north near the transform.

primary diking event) occurred within 6 h on 22 January. During this time there is a 2-h period where *T* wave detection rates exceed levels during other parts of the day by a factor of 3 to 7. Most of these detections, however, were recorded only on the northern two hydrophones, which are positioned ~550 and 1,100 km from the eruption site (Figure 1b). Arrivals on one or both of the central hydrophones were identified for 20 earthquakes that occurred on 22 January, allowing their locations to be determined. Of these, 18 earthquakes took place during the period of most intense activity between 1500 and 1600 UT.

[15] Earthquakes on 22 January are all located within a 35-km-long area to the north and south of 9°50′N site, extending several kilometers past the section of ridge crest where recent lava flows were observed (Figure 4) [*Soule et al.*, 2007]. The hydroacoustic earthquake data set does not clearly indicate earthquake migration; however, seismicity does take place in discrete time clusters, occurring in succession from north to south, then back to the north of 9°50′N site within the 1-h time period.

[16] The earthquakes detected by the hydrophones are likely the largest events produced during the eruption. Using a cylindrical-spreading transmission loss model, we estimate acoustic source levels of 202–218 dB (re 1μPa @ 1 m) for these events, equivalent to seismic magnitudes of ~2–3.5 m_b [*Bohnenstiehl et al.*, 2002]. None of the 22 January earthquakes were located by land-based seismic stations (ISC catalog), further constraining the maximum earthquake sizes to be less than m_b 4–4.5 [*Bohnenstiehl and Tolstoy*, 2003]. Those earthquakes large enough to be located using the hydrophone data appear to occur at the distal ends of the magma injection event [cf. *Rubin*, 1990]. Scaling relationships for normal faulting earthquakes [*Scholz*, 2002] suggest that these largest ruptures have a physical diameter of 0.15–0.5 km, or 10–30% of the AMC depth.

[17] The *T* wave signal risetime also was measured for all detected and located earthquakes recorded from 9°50′N during January 2006 (Figure 5). Risetime is the time interval between the initial appearance of the *T* wave signal packet above ambient noise and the time of peak energy [*Schreiner et al.*, 1995]. A decrease in risetimes to <5 s has been interpreted as shoaling of the magma dike during intrusion events at the Juan de Fuca Ridge [*Dziak et al.*, 2007], where very short risetimes imply actual magma eruption onto the seafloor. The short risetimes beginning after 1500 UT on 22 January, in addition to the overall high seismic activity, are interpreted as evidence of

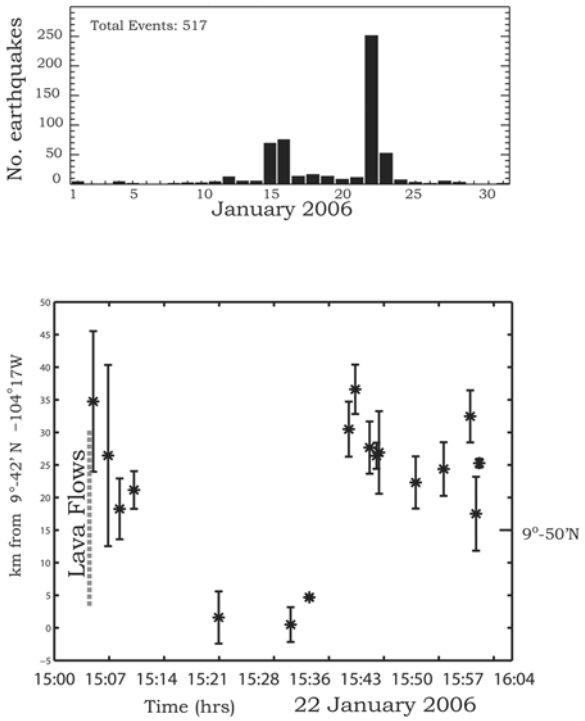

Figure 4. (top) Histogram of earthquake counts during the 3 week period in January 2006, recorded on the northwest hydrophone. Only 20 of these detections can be accurately located (Figure 1). No earthquakes were detected during other times. (bottom) Time-distance diagram of earthquakes located at EPR from 1500 to 1600 UT on 22 January 2006. Dashed line shows along-axis length of lava flows that occurred during the eruption [*Soule et al.*, 2007]. The inferred starting location of the dike is 9°50′N [*Tolstoy et al.*, 2006]. Vertical bar shows the mean 1-sigma uncertainty in locations.

a seafloor eruption on this day. In performing the risetime analysis, we use all detected *T* waves and make the assumption that those events too small to be accurately located are spatially clustered with the 18 earthquakes located during this period.

[18] The short risetimes during 12 and 15–16 January imply shallow faulting and suggest possible seafloor eruptions on these days as well. Local increases in seismic activity on the OBS data also were observed during 0400–0500 UT on 12 January and during 15–16 January; however, the scale of activity on these days is significantly less than that observed on 22 January [*Tolstoy et al.*, 2006]. Unfortunately, earthquakes from 12 and 15–16 January were very low magnitude and only recorded on two hydrophones. Consequently, it is impossible to determine precise locations for these events or investigate their spatial relationships in detail.

4.2. EPR Flank/Clipperton Transform Seismicity

[19] At 0721 UT on 23 January 2006, ~15 h after the last earthquake occurred on the ridge crest, a sequence of 16 earthquakes began either on (because of location uncertainty) the eastern flank of the ridge segment to the north of 9°50′N or along the western Clipperton Transform. This is a region known to be seismically active on the basis of the long-term AUH monitoring (Figure 1). Only one of the events within the post eruption sequence was of sufficient size to be located by global seismic networks. This second event within the series has a magnitude of m_b 4.0 (On-Line Bulletin, International Seismic Centre, Thatcham, U. K., 2007, available at http://www.isc.ac.uk). Activity in the vicinity of the Clipperton Transform subsided to background levels after approximately 1 week.

[20] Risetimes for these Clipperton earthquakes were also calculated (Figure 5) and are typically >10 s for the majority of events. In contrast, almost all of the seismicity from 22 January is <10 s. Given that previously documented dike intrusion events typically exhibit short risetimes (<5 s), we interpret the inside corner seismicity as likely tectonic in origin and not caused by nearby magma intrusion in the 10°10′N segment.

[21] As local seismicity rates fall during the posteruption period, regional *P*, *S* and *T* arrivals can be identified on the 9°50′N ocean bottom seismic stations. To verify the location of these events we used the time differences between the impulsive S and P arrivals on the OBSs to independently estimate event-to-stations distances for the 16 hydrophone located events. The results show consistency with the hydrophone-derived epicenters, with S-P times clustering between 3 and 4 s. For a standard ocean crustal model, with a V_p/V_s ratio 1.7 ± 0.1, this corresponds to hypocentral distances of ~25–40 km from the OBS stations. Most events within the sequence therefore lie to the south of the transform; yet, this activity is spatially distinct from that which occurred on 22 January.

[22] Although bathymetry may influence absolute *T* wave locations, the hydrophone array routinely locates events on the western inside corner of the Clipperton Transform (Figure 1). Consequently, any assumption that this post 22 January seismicity has been incorrectly located to the east of the ridge crest would also imply that the 10°05′ to 10°10′N section of the ridge axis has been active over the

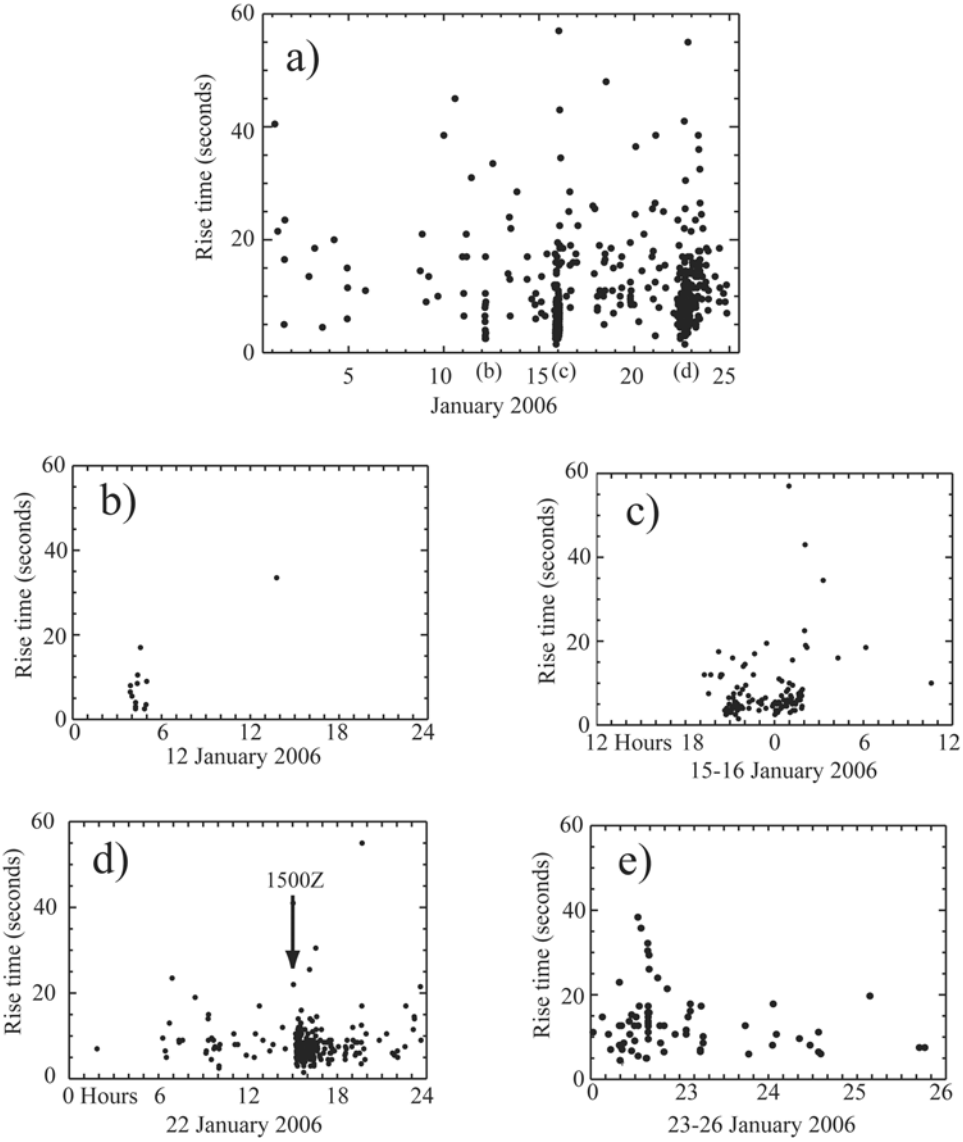

Figure 5. (a) Diagram of earthquake *T* wave risetimes from all EPR events detected during January 2006. Clustering of short-risetime *T* wave arrivals (<5 s) have been interpreted as resulting from shallow focus earthquakes and correlated to seafloor eruption sites during previous diking episodes. (b–d) Details of short risetimes from 12, 15–16, and 22 January, respectively. The short risetimes and high seismic activity on 22 January are interpreted as evidence of a seafloor eruption, consistent with *Tolstoy et al.* [2006]. The short risetimes during 12 and 15–16 January also imply shallow faulting and possible seafloor extrusive events on these days; however, these events are too small to be accurately located. (e) The risetime from earthquakes near the Clipperton that occurred between 23 and 26 January. The risetimes for the majority of these events are >10 s, consistent with seismicity caused by tectonic, rather than magmatic, processes.

last decade. Given the dearth of *T* wave events located along other portions of the EPR, this behavior would be highly anomalous.

5. Evaluation of Past, Probable EPR Volcanic Swarms

[23] An unresolved question in the study of mid-ocean ridges is the recurrence rate of dike intrusion events, particularly along the fast spreading East Pacific Rise where we might expect relatively frequent (1/decade) seafloor spreading events along any given section of the ridge. Now that a dike intrusion and seafloor eruption at 9°50′N has been confirmed, review of our 11-year hydroacoustic earthquake database was performed using a single-link cluster (SLC) analysis [*Davis and Frohlich*, 1991] to find similar spatially and

Table 1. Date and Location of EPR Hydrophone Detected Earthquake Swarms

Map Number	Latitude (°N, S)	Longitude (°W)	Start Date and Time (UT)	Number of Located Events	Duration (hours)
1	3.41	−102.22	28 May 1996 0340	69	171.07
2	1.81	−102.31	14 Jun 1996 1247	4	4.22
3	5.44	−102.45	4 May 1997 2040	4	1.5
4	1.71	−102.27	6 Jun 1997 2236	33	64.08
5	−5.35	−106.56	25 Jun 1997 1248	6	5.97
6	1.94	−102.14	5 Aug 1997 1600	10	19.72
7	−2.99	−102.59	3 Sep 1997 2110	11	50.07
8	−2.95	−102.61	18 Jun 1998 1933	5	53.12
9	−1.21	−102.49	26 Jun 1998 0451	5	2.12
10	2.42	−102.11	3 Jul 1998 1525	9	7.03
11	−3.81	−104.01	16 Oct 1998 0159	11	2.42
12	1.94	−102.14	22 May 1999 1253	18	30.38
13	−5.42	−106.56	27 May 1999 0909	72	48.52
14	7.24	−102.71	28 Jul 1999 0300	9	0.93
15	1.94	−102.20	21 Sep 2000 0743	5	6.52
16	−6.20	−106.97	24 Dec 2000 1102	5	3.12
17	8.67	−104.22	2 Mar 2001 0313	25	8.12

temporally sized swarms along the rest of the EPR. The search method uses a metric of the summed root-square of the inferred eruption earthquake rate (18 events in 1 h = 0.3 eq/min) and along ridge distance (18 events over 40 km = 0.45 eq/km) as detected on the regional hydrophone array. The SLC analysis was performed on the entire 11-year EPR earthquake database, although a 2-year gap exists between December 2002 and December 2004, when four of the six instruments failed to record data because of a microprocessor and hard drive communication problem.

[24] A total of 17 individual swarms were identified as having similar space-time distributions as the January 2006 dike intrusion event (Table 1 and Figure 6). Their durations range from approximately 1 h to near 3 days, with between 4 and 73 earthquakes located within the catalog. The majority of these identified swarms occurred at ~2°N, where the EPR and Galapagos Rift intersect, and four of the swarms (2,3,4, and 11) occur at overlap zones between ridge segments (Table 1).

6. Discussion

[25] Our array of autonomous hydrophones moored along the flanks of the East Pacific Rise recorded seismicity associated with the January 2006 dike intrusion event at 9°50′N at regional (~500–1200 km) distances. The hydrophones detected 255 and 252 earthquakes prior to and during the inferred eruption day of 22 January, whereas the in situ OBS array was detecting >1000 events per day [*Tolstoy et al.*, 2006]. Although preliminary age estimates have suggested significant volumes of lava may have been extruded as early as the fall of 2005 [*Rubin et al.*, 2008], regional hydrophone observations, which are sensitive to M > 2.0–2.5 earthquakes in this setting, show no indication of swarm activity during this period.

[26] Of the 252 detected events, 20 earthquakes were large enough to be recorded on 3 or 4 hydrophones and an epicenter location could be derived. Of these, 18 earthquakes occurred within 1 h at 1500 UT on 22 January, consistent with the time of the seafloor eruption inferred from the OBS data. The short risetimes of *T* wave events on 22 January also are consistent with a seafloor eruption on this day. However, the short risetimes during 12 and 15–16 January imply shallow faulting and possible seafloor eruption on these days as well. Unfortunately, a well-constrained location could not be derived for earthquakes from 12 and 15–16 January since the events were not large enough to be recorded on 3+ hydrophones. Nonetheless, their temporal clustering with the located events on 22 January suggests that they lie along the 9°40′–10°00′N ridge crest, as opposed to the transform or inside corner region.

[27] Despite the relatively small number of large earthquakes located on 22 January, the events do show a change in their locations along the ridge axis that is likely caused by the movement of magma in the shallow ocean crust. The events locate in clusters that change location from north

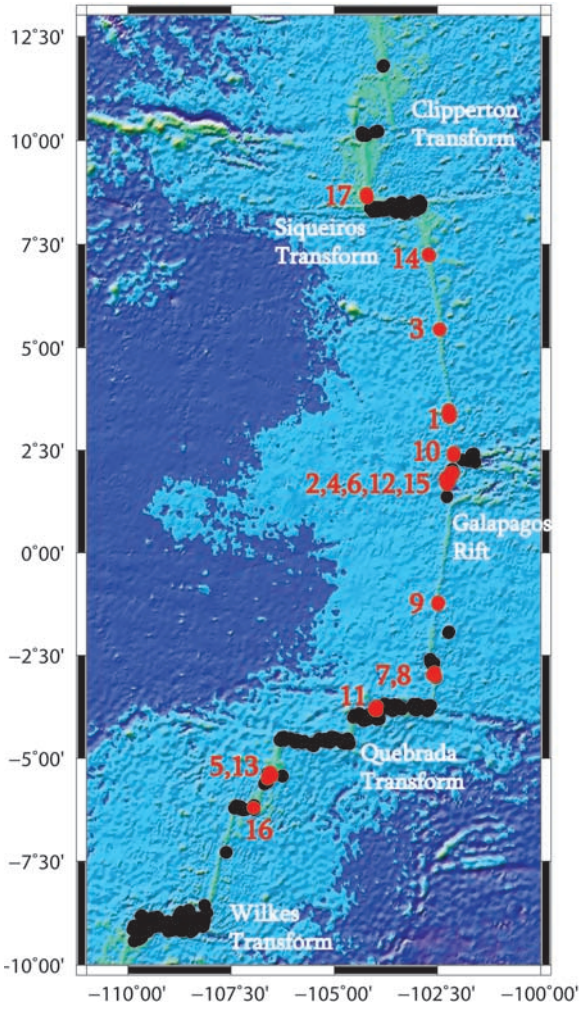

Figure 6. A single-link cluster analysis was used to identify EPR earthquake swarm clusters with similar space-time distribution as the January 2006 eruption swarm at 9°50′N. A total of 17 swarms (red dots) were identified; source information is listed in Table 1. Black dots show all earthquakes located using the EPR hydrophone array from May 1996 to January 2006.

of 9°50′N, to south of 9°50′N, back to north covering a spatial distance of ∼35 km over the time period of 1 h. The hydrophone-detected earthquakes occur at the distal ends of the magma injection event, which exhibited the greatest volume of erupted lava near 9°50′N [*Tolstoy et al.*, 2006; *Soule et al.*, 2007]. The clustering of seismic events in these regions mark the propagation of the dike away from a local high in ridge axis elevation and cross-sectional area [*Scheirer and Macdonald*, 1993] and presumably into thicker sections of brittle crust that can support larger earthquakes sizes [*Rubin*, 1990]. Most of located events on 22 January cluster to the north of the eruptive area, near an inflationary (cross-sectional area) minimum near 9°55′N (Figure 1) [*Scheirer and Macdonald*, 1993].

[28] The progressive migration of earthquake activity at slower spreading rate ridges [e.g., *Dziak et al.*, 2007] and within other rift zones [e.g., *Einarsson and Brandsdottir*, 1980; *Klein*, 1987] has been interpreted as tracking the lateral propagation of a dike away from a central magma reservoir. If the dike is assumed to originate near 9°50′N [*Tolstoy et al.*, 2006; *Soule et al.*, 2007] the clustering of hydrophone-located events to the north and south implies a bilateral direction of propagation. This may have occurred via simultaneous injection to the north and the south or during discrete episodes lasting ∼5–20 min and separated by ∼5–10 min (Figure 4).

[29] The injection of magma bilaterally along rift zones has not been observed at the Juan de Fuca Ridge, although it has been observed twice (December 1974 and March 1980) during the Krafla rifting episode in Iceland [*Buck et al.*, 2006]. At Krafla, the north then south injection of magma occurred over a 2 h time span and covered a distance of 11 km, consistent with the timing of the EPR intrusion event although covering roughly a third of the distance. The dual injection directions were interpreted as a result of the similarity between pressure in the magma chamber and the northward driving pressure, defined as the difference between magma pressure and tectonic stress at the dike tip. Regional tectonic stress, accumulated over previous dike injections, prevented further northward intrusion however the elevated pressure in the magma chamber managed to force the dike southward (B. Brandsdottir, personal communication, 2008). If the dike had not propagated south, either deflation at Krafla would have ceased or the dike would have erupted within or near the caldera.

[30] If we assume the first *T* wave activity just to the north of the 9°50′N site marks the initiation of a dike that propagates simultaneously to the south and north (Figure 4), this requires very high rates of ∼31.5 m s^{-1} (southward) and ∼13.8 m s^{-1} (northward). *Tolstoy et al.* [2006], however, reported that elevated seismic activity began at ∼1345 UT on the OBS array near 9°50′N, roughly 96 min before the first earthquakes occur 17 km down-rift to the south. This time difference yields a propagation rate in both directions of ∼2.9–3.0 m s^{-1}. Or, using the onset time of more intense activity (1445 UT), which *Tolstoy et al.* [2006] interpreted to mark the vertical rise of a dike

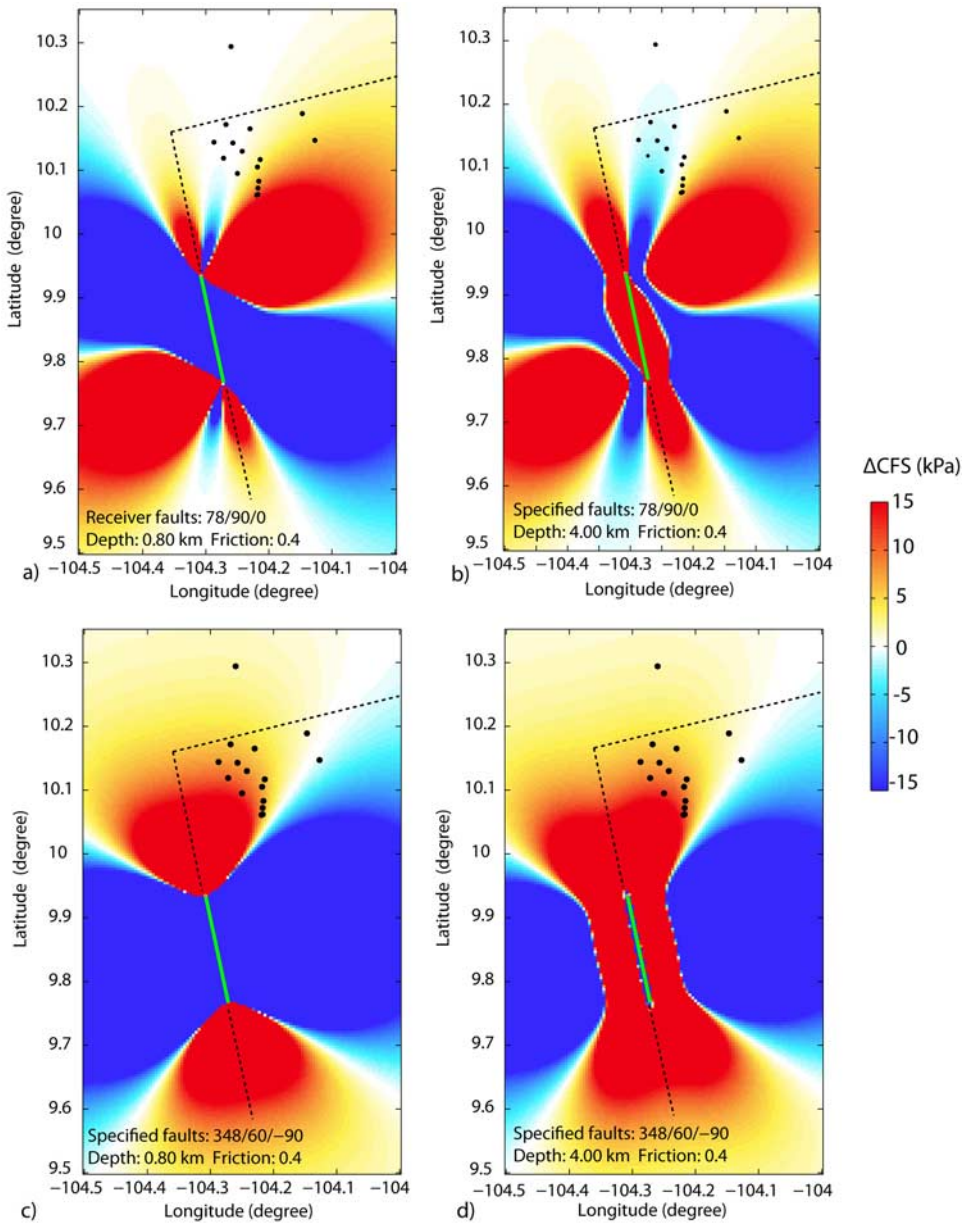

Figure 7. Coulomb stress change using a dike 1.5 km tall (constrained from MCS studies) with 1 m uniform opening extending from 9°46′ to 9°56′N. (a and b) A left-lateral strike-slip receive fault (i.e., the transform) and (c and d) ridge-parallel normal faults dipping at 60°. Depths of 0.8 km (dike level) and 4 km are shown for both cases.

beneath the 9°50′N vent field, we estimate a southward propagation rate of 7.9 m s^{-1}. These estimates, however, are all ∼10–100 times greater than the maximum injection speeds observed from slow and intermediate rate ridges [e.g., *Dziak et al.*, 2007].

[31] Alternatively, differences in magma storage beneath a fast spreading ridge, relative to other rift zones, could facilitate differences in the style of dike emplacement. Multichannel seismic studies show a reflection from an axial magma lens at ∼1.5 ± 0.3 km depth beneath >60% of the ridge axis at fast spreading rates [*Carbotte*, 2001]. Locally, between 9°03′N overlapper and the Clipperton transform, this percentage may be even higher, with a nearly continuous AMC reflector observed when the axis was surveyed in 1985 [*Detrick et al.*, 1987]. Therefore magma does not have to be transported laterally to erupt down rift; rather, it can rise vertically from below. A dike (mode I crack) initiating along one section of the axis, creates a near instantaneous static stress change that works to promote tensile failure and

dike emplacement from a magma lens located down-rift and aligned with the original dike [e.g., *Bohnenstiehl et al.*, 2004a]. In this scenario, multiple dikes become activated along the rift zone, as opposed to a single dike that propagates from a central point transporting melt down rift and potentially tapping the underlying AMC as it progresses. As the last eruption along the 9°46′–9°56′N section of the axis took place in 1991, extensional stresses are expected to have built up to levels near failure [e.g., *Rubin*, 1995; *Buck et al.*, 2006], potentially making the system sensitive to even small stress perturbations.

[32] Approximately 15 h after the last earthquake occurred on the ridge crest, a sequence of 16 earthquakes began on the eastern flank of the ridge segment to the north of 9°50′N and along the western Clipperton Transform. The potential for elastic interactions between spreading centers and oceanic transforms has been noted previously [*Forsyth et al.*, 2003; *Bohnenstiehl et al.*, 2004b; *Gregg et al.*, 2006]. To investigate the close spatiotemporal proximity of this activity to the diking event, a boundary element model is used to estimate the static stress changes induced by the intrusion. The modeled dike extends along the length of the young lava flows observed by *Soule et al.* [2007] (9°46′–9°56′N) and is assumed to be 1.5 km tall, with a 1 m uniform opening (inferred from ophiolites [e.g., *Kidd*, 1977; *Gillis*, 2001]). In Figure 7, changes in Coulomb Failure Stress (ΔCFS) [e.g., *Stein*, 1999] are calculated for two sets of receiver faults: left-lateral strike-slip faults, representing the transform, and ridge-parallel normal faults dipping at 60°, representing abyssal faults within the inside corner region. Depths of 0.8 km (dike level) and 4 km are shown for both cases. Positive ΔCFS values (red) represent regions where failure is promoted by the diking event; negative ΔCFS values (blue) indicate regions where failure is inhibited.

[33] Although left-lateral slip is enhanced along much of the transform, dike emplacement leads to negative ΔCFS near the ridge transform intersection. Consequently only ~50% of the epicenters lie within the region of encouraging stress change (Figure 7a). In contrast, the seismically active zone lies entirely within the zone of positive ΔCFS for ridge-parallel normal faulting, again consistent with the reactivation of the inside corner area (Figure 7b). As stress changes scale primarily with the height of the dike [*Rubin and Pollard*, 1988], ΔCFS within the vicinity of these epicenters is only ~1–10 kPa. Although small in magnitude, similar static stress changes have been shown to trigger seismicity in terrestrial studies [*Ziv and Rubin*, 2000]. Moreover, *Stroup et al.* [2007] have shown evidence for the semidiurnal triggering of microearthquakes ($M_L < 2$) at the 9°50′N site in response to transient tidal stresses possibly as small as 1 kPa. Therefore, even though the inferred ΔCFS changes are relatively small, the stress change model due to ridge dike intrusion is consistent with the triggering of ridge-parallel normal faulting within the inside corner. Moreover, there is not necessarily a different crustal stress mechanism that resulted in both the 23 January 2006 seismicity and the 1996–2005 background Clipperton earthquakes. The static stress changes associated with the 2006 dike simply add to the existing stress field, and drive the already active faults closer to failure, resulting in heightened Clipperton earthquake activity following the dike intrusion.

[34] A single-link cluster method was used to review the entire EPR hydrophone earthquake database from 1996 to 2006 for earthquake swarms with similar space-time event distributions as the January 2006 dike intrusion event. The database is not complete, however, since a data gap exists during the years from December 2002 to December 2004. A total of 17 swarms were identified as having similar spatiotemporal patterns as the 2006 dike event, and all of the swarms meeting these criteria occurred prior to 2002. Three of the 1996–1999 swarm sites (4, 8, and 10) were surveyed several years later during a response cruise [*Fornari et al.*, 2000]; however, evidence for very recent magmatic activity was inconclusive because of the age of sites. A CTD survey performed at the 2 March 2001 earthquake swarm site at 8°40′N did discover a hydrothermal plume of dissolved manganese [*Bohnenstiehl et al.*, 2003], providing the only other location where earthquake activity could be associated with recent hydrothermal/magmatic activity at the EPR other than at 9°50′N. As has been shown during seafloor spreading events at the Juan de Fuca Ridge [*Dziak et al.*, 2007], surveying ridge crest earthquake swarm sites several years after they were detected significantly decreases the probability that seafloor magmatic and hydrothermal evidence will be found.

7. Conclusions

[35] The findings presented here are consistent with the interpretations of *Tolstoy et al.* [2006] that a significant seafloor eruption at 9°50′N

likely occurred during a dike intrusion event on 22 January 2006. Admittedly, sound channel hydrophones at regional distances provide an incomplete picture of the seismic activity at 9°50′N because of the inability to detect small magnitude (M_L < 2) events typically associated with dike intrusion activity at the ridge crest. However, the dike intrusion dynamics inferred from the available hydroacoustic data suggest that diking may have initiated along the entire length of the eruptive zone (9°46′–9°56′N), or slightly beyond, within a period of only 1–2 h.

[36] Short-risetime events are observed on 22 January, as well as on 12 and 15–16 January. Although the activity on 12 and 15–16 January cannot be accurately located, its temporal clustering with the 22 January activity suggest that it may represent a preparatory phase of shallow faulting and possibly extrusion. Temperature records from high-temperature "M" Vent at 9°51.6′N show a dramatic >208°C, 17-day decrease in vent fluid temperature beginning on 11 January, consistent with a major change in hydrothermal fluid circulation prior to the 22 January eruption (Von Damm et al., manuscript in preparation, 2009). Hydroacoustic observations show no indication of 9°50′N swarm activity during the summer or fall of 2005, when radiometric evidence indicates that a significant volume of lava effusion occurred [*Rubin et al.*, 2008]. This suggests fast spreading eruptions may take place without producing seismic signals larger than the M_L > 2.0–2.5 detection threshold of the regional array.

[37] Given confirmation of a seafloor eruption associated with January 2006 earthquake swarm, a search of the existing hydroacoustic earthquake catalog (that dates back to 1996) finds 17 similar swarms. Many of these swarms appear to be located near ridge offsets, suggesting that the generation of M_L > 2.5 earthquakes along the EPR is favored in areas where the brittle layer thickens along axis. This is consistent with the clustering of hydrophone detected events away from the 9°50′N site, an area where the high density of high-temperature vent systems [*Fornari et al.*, 2004], increased eruptive volume [*Soule et al.*, 2007] and the presence of subaxial melt anomalies [*Toomey et al.*, 2007] suggest that the brittle crust is locally warmer and thinner.

Acknowledgments

[38] The authors would like to thank S. Carbotte, R. Reves-Sohn, and an anonymous reviewer for constructive edits to the manuscript. The authors also wish to thank T. K. Lau for programming assistance, S. Merle for assistance with Figure 1, and the PMEL/EDD for engineering and logistical support. The authors also wish to thank B. Brandsdottir for very helpful discussions. This study was funded by NSF grants OCE-9811575, OCE-0137164, and OCE-0201692. This paper is NOAA/PMEL contribution 3264.

References

Baker, E. T., G. J. Massoth, R. A. Feely, R. W. Embley, and R. E. Thomson (1995), Hydrothermal event plumes from the CoAxial seafloor eruption site, Juan de Fuca Ridge, *Geophys. Res. Lett.*, *22*, 147–150, doi:10.1029/94GL02403.

Bohnenstiehl, D. R., and M. Tolstoy (2003), Comparison of teleseismically and hydroacoustically derived earthquake locations along the north-central Mid-Atlantic Ridge and Equatorial East Pacific Rise, *Seismol. Res. Lett.*, *74*(6), 791–802.

Bohnenstiehl, D. R., M. Tolstoy, R. P. Dziak, C. G. Fox, and D. K. Smith (2002), Aftershocks in the mid-ocean ridge environment: An analysis using hydroacoustic data, *Tectonophysics*, *354*, 49–70, doi:10.1016/S0040-1951(02)00289-5.

Bohnenstiehl, D. R., et al. (2003), Anomalous seismic activity at 8°37–42′N on the East Pacific Rise: Hydroacoustic detection and site investigation, *RIDGE 2000 Events*, *1*, 18–20.

Bohnenstiehl, D. R., R. P. Dziak, M. Tolstoy, C. G. Fox, and M. Fowler (2004a), Temporal and spatial history of the 1999–2000 Endeavour Segment seismic series, Juan de Fuca Ridge, *Geochem. Geophys. Geosyst.*, *5*, Q09003, doi:10.1029/2004GC000735.

Bohnenstiehl, D. R., M. Tolstoy, and E. Chapp (2004b), Breaking into the plate: A 7.6 Mw fracture-zone earthquake adjacent to the Central Indian Ridge, *Geophys. Res. Lett.*, *31*, L02615, doi:10.1029/2003GL018981.

Buck, W. R., P. Einarsson, and B. Brandsdottir (2006), Tectonic stress and magma chamber size as controls on dike propagation: Constraints from the 1975–1984 Krafla rifting episode, *J. Geophys. Res.*, *111*, B12404, doi:10.1029/2005JB003879.

Carbotte, S. M. (2001), Mid-ocean ridge seismic structure, in *Encyclopedia of Ocean Sciences*, edited by J. H. Steele, S. A. Thorpe, and K. K. Turekian, pp. 1220–1228, Academic, London.

Cowen, J. P., et al. (2007), Volcanic eruptions at East Pacific Rise near 9°50′N, *Eos Trans. AGU*, *88*, 81–83, doi:10.1029/2007EO070001.

Davis, S. D., and C. Frohlich (1991), Single-link cluster analysis, synthetic earthquake catalogues, and aftershock identification, *Geophys. J. Int.*, *104*, 289–306, doi:10.1111/j.1365-246X.1991.tb02512.x.

Detrick, R. S., P. Buhl, E. Vera, J. Mutter, J. Orcutt, J. Madsen, and T. Brocher (1987), Multichannel seismic imaging of a crustal magma chamber along the East Pacific Rise between 9°N and 13°N, *Nature*, *326*, 35–41, doi:10.1038/326035a0.

Dziak, R. P., C. G. Fox, and A. E. Schreiner (1995), The June–July 1993 seismo-acoustic event at CoAxial segment, Juan de Fuca Ridge: Evidence for a lateral dike injection, *Geophys. Res. Lett.*, *22*(2), 135–138, doi:10.1029/94GL01857.

Dziak, R. P., D. R. Bohnenstiehl, H. Matsumoto, C. G. Fox, D. K. Smith, M. Tolstoy, T. K. Lau, J. H. Haxel, and M. J. Fowler (2004), *P*- and *T*-wave detection thresholds, *Pn* velocity estimate, and detection of lower mantle and core *P*-waves on ocean sound-channel hydrophones at the Mid-

Atlantic Ridge, *Bull. Seismol. Soc. Am.*, *94*, 665–677, doi:10.1785/0120030156.

Dziak, R. P., D. R. Bohnenstiehl, J. P. Cowen, E. T. Baker, K. H. Rubin, J. H. Haxel, and M. J. Fowler (2007), Rapid dike injection leads to volcanic eruptions and hydrothermal plume release during seafloor spreading events, *Geology*, *35*, 579–582, doi:10.1130/G23476A.1.

Einarsson, P., and B. Brandsdottir (1980), Seismological evidence for lateral magma intrusion during the July 1978 deflation of Krafla Volcano in NE Iceland, *J. Geophys.*, *47*, 160–165.

Fornari, D. J., T. Shank, K. L. Von Damm, T. K. P. Gregg, M. Lilley, G. Levai, A. Bray, R. M. Haymon, M. R. Perfit, and R. Lutz (1998), Time-series temperature measurements at high-temperature hydrothermal vents, East Pacific Rise 9°49′–51′N: Evidence for monitoring a crustal cracking event, *Earth Planet. Sci. Lett.*, *160*, 419–431, doi:10.1016/S0012-821X(98)00101-0.

Fornari, D., M. Perfit, M. Tolstoy, and AHA-Nemo2 Scientific Party (2000), Investigation of autonomous hydrophone array event sites on the East Pacific Rise crest near 3 20′N and 1 45′N and on the Galapagos Rift at 97.5W, *Eos Trans. AGU*, *81*(48), Fall Meet. Suppl., Abstract T51D-09.

Fornari, D. J., et al. (2004), Submarine lava flow emplacement at the East Pacific Rise 9°50′N: Implications for uppermost ocean crust stratigraphy and hydrothermal fluid circulation, in *Mid-Ocean Ridges: Hydrothermal Interactions Between the Lithosphere and Oceans*, *Geophys. Monogr. Ser.*, vol. 148, edited by C. R. German, J. Lin, and L. M. Parson, pp. 187–217, AGU, Washington, D. C.

Forsyth, D. W., Y. Yang, M.-D. Mangriotis, and Y. Shen (2003), Coupled seismic slip on adjacent oceanic transform faults, *Geophys. Res. Lett.*, *30*(12), 1618, doi:10.1029/2002GL016454.

Fox, C. G., W. E. Radford, R. P. Dziak, T. Lau, H. Matsumoto, and A. E. Schreiner (1995), Acoustic detection of a seafloor spreading episode on the Juan de Fuca Ridge using military hydrophone arrays, *Geophys. Res. Lett.*, *22*(2), 131–134.

Fox, C. G., H. Matsumoto, and T.-K. A. Lau (2001), Monitoring Pacific Ocean seismicity from an autonomous hydrophone array, *J. Geophys. Res.*, *106*(B3), 4183–4206, doi:10.1029/2000JB900404.

Gillis, K. M. (2001), New insights into the creation and evolution of the oceanic lithosphere gained from ocean drilling, *Geosci. Can.*, *28*, 163–170.

Gregg, P. M., J. Lin, and D. K. Smith (2006), Segmentation of transform systems on the East Pacific Rise: Implications for earthquake processes at fast-slipping oceanic transform faults, *Geology*, *34*, 289–292, doi:10.1130/G22212.1.

Haymon, R., et al. (1993), Volcanic eruption of the mid-ocean ridge along the East Pacific Rise at 9°45–52′N: Direct submersible observation of seafloor phenomena associated with an eruption event in April, 1991, *Earth Planet. Sci. Lett.*, *119*, 85–101, doi:10.1016/0012-821X(93)90008-W.

Kidd, R. G. W. (1977), A model for the process of formation of the upper oceanic crust, *Geophys. J. R. Astron. Soc.*, *50*(1), 149–183.

Klein, F. (1987), The seismicity of Kilauea's magma system, in *Volcanism in Hawaii*, edited by R. W. Decker, T. L. Wright, and P. H. Stauffer, *U.S. Geol. Surv. Prof. Pap.*, *1350*, 1019–1086.

Park, M.-K., and R. Odom (2001), Modal scattering: A key to understanding oceanic T-waves, *Geophys. Res. Lett.*, *28*(17), 3401–3404.

Rubin, A. M. (1990), A comparison of rift-zone tectonics in Iceland and Hawaii, *Bull. Volcanol.*, *52*, 302–319, doi:10.1007/BF00304101.

Rubin, A. M. (1995), Propagation of magma-filled cracks, *Annu. Rev. Earth Planet. Sci.*, *23*, 287–336, doi:10.1146/annurev.ea.23.050195.001443.

Rubin, A. M., and D. D. Pollard (1988), Dike-induced faulting in rift zones of Iceland and Afar, *Geology*, *16*, 413–417, doi:10.1130/0091-7613(1988)016<0413:DIFIRZ>2.3.CO;2.

Rubin, K. H., M. Tolstoy, D. J. Fornari, R. P. Dziak, F. Waldhauser, and K. L. Von Damm (2008), Integrating radiometric, geophysical, and thermal signals of volcanic unrest and eruption in 2005–06 at 9°50′N EPR, *Eos Trans. AGU*, *89*(53), Fall Meet. Suppl., Abstract B23F-07.

Scheirer, D. S., and K. C. Macdonald (1993), Variation in cross-sectional area of the axial ridge along the East Pacific Rise: Evidence for the magmatic budget of a fast-spreading center, *J. Geophys. Res.*, *98*, 7871–7885, doi:10.1029/93JB00015.

Scholz, C. H. (2002), *The Mechanics of Earthquakes and Faulting*, 2nd ed., 496 pp., Cambridge Univ. Press, Cambridge, U. K.

Schreiner, A. E., C. G. Fox, and R. P. Dziak (1995), Spectra and magnitude of T-waves from the 1993 earthquake swarm on the Juan de Fuca Ridge, *Geophys. Res. Lett.*, *22*, 139–142, doi:10.1029/94GL01912.

Sohn, R. A., D. J. Fornari, K. L. Von Damm, J. A. Hildebrand, and S. C. Webb (1998), Seismic and hydrothermal evidence for a cracking event on the East Pacific Rise crest at 9°50′N, *Nature*, *396*, 159–161, doi:10.1038/24146.

Soule, S. A., D. J. Fornari, M. R. Perfit, and K. H. Rubin (2007), New insights into mid-ocean ridge volcanic processes from the 2005–06 eruption of the East Pacific Rise, 9°46′–56′N, *Geology*, *35*(12), 1079–1082, doi:10.1130/G23924A.1.

Stein, R. S. (1999), The role of stress transfer in earthquake occurrence, *Nature*, *402*, 605–609, doi:10.1038/45144.

Stroup, D., D. R. Bohnenstiehl, M. Tolstoy, F. Waldhauser, and R. T. Weekly (2007), The pulse of the seafloor: Tidal triggering of microearthquakes at 9°50′N East Pacific Rise, *Geophys. Res. Lett.*, *34*, L15301, doi:10.1029/2007GL030088.

Tolstoy, M., D. Bohnenstiehl, M. Edwards, and G. Kurras (2001), The seismic character of volcanic activity at the ultra-slow spreading Gakkel Ridge, *Geology*, *29*, 1139–1142.

Tolstoy, M., et al. (2006), A seafloor spreading event captured by seismometers: Forecasting and characterizing an eruption, *Science*, *314*, 1920–1922, doi:10.1126/science.1133950.

Tolstoy, M., F. Waldhauser, D. R. Bohnenstiehl, R. T. Weekly, and W.-Y. Kim (2008), Seismic identification of along-axis hydrothermal flow on the East Pacific Rise, *Nature*, *451*, 181–184, doi:10.1038/nature06424.

Toomey, D. R., D. Jousselin, R. A. Dunn, W. S. D. Wilcock, and R. S. Detrick (2007), Skew of mantle upwelling beneath the East Pacific Rise governs segmentation, *Nature*, *446*, 409–414, doi:10.1038/nature05679.

Ziv, A., and A. M. Rubin (2000), Static stress transfer and earthquake triggering: No lower threshold in sight?, *J. Geophys. Res.*, *105*, 13,631–13,642, doi:10.1029/2000JB900081.